Progress in Natural Science: Materials International 28 (2018) 178–182

Contents lists available at ScienceDirect

Progress in Natural Science: Materials International

journal homepage: www.elsevier.com/locate/pnsmi

Original Research

Reducing Zn diffusion in single axial junction InP nanowire solar cells for improved performance

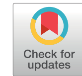

Ziyuan Li[a], Inseok Yang[a], Li Li[b], Qian Gao[a], Jet Shoon Chong[a], Zhe Li[c], Mark N. Lockrey[b], Hark Hoe Tan[a], Chennupati Jagadish[a], Lan Fu[a,*]

[a] *Department of Electronic Materials Engineering, Research School of Physics and Engineering, The Australian National University, Canberra, ACT 2601, Australia*
[b] *Australian National Fabrication Facility, The Australian National University, Canberra, ACT 2601, Australia*
[c] *Department of Applied Mathematics, Research School of Physics and Engineering, The Australian National University, Canberra, ACT 2601, Australia*

ARTICLE INFO

Keywords:
InP
Nanowire solar cells
Axial junction
Selective-area MOVPE
CL
EBIC

ABSTRACT

In this work axial n-i-p junction InP nanowires were grown by selective-area metal organic vapor phase epitaxy (SA-MOVPE) technique with the growth sequence starting from n-segment. The optical properties and carrier lifetimes of the n-, i- and p-type segments were studied and compared using time-resolved photoluminescence (PL) and cathodoluminescence (CL) measurements. We demonstrate for the first time that CL is capable of resolving the electrical profile of the nanowires, namely the varied lengths of the n-, i- and p-segments, providing a simple and effective approach for nanowire growth calibration and optimization. The CL result was further confirmed by electron beam induced current (EBIC) and photocurrent mapping measurements performed from the fabricated single nanowire solar cell devices. It is revealed that despite a non-optimized device structure (very long n-region and short i-region), the n-i-p nanowire solar cells show improved power conversion efficiency (PCE) than the previously reported p-i-n (growth starts with p-segment) single nanowire solar cells due to reduced p-type dopant (Zn) diffusion during the growth of n-i-p solar cell structure.

1. Introduction

III-V semiconductor nanowires have been studied intensively in recent years as promising candidates for optoelectronic applications such as lasers [1,2], photodetectors [3,4], light-emitting diodes (LEDs) [5,6] and solar cells [7–9]. For solar cell applications, due to their suitable bandgaps, superior optical and electrical properties, and small footprints, III-V compound semiconductor based nanowire solar cells have shown great promise in achieving high power conversion efficiency (PCE) with much reduced material cost. To date InP and GaAs nanowire array solar cells fabricated by bottom-up approach have been reported with the record efficiencies of 13.8% and 15.3%, respectively [8,9]. Top-down approaches also lead to a record efficiency as high as 17.8% [10]. However, these experimentally reported solar cell efficiencies are far below theoretical predictions, for instance, ~ 32.5% for bandgap at ~ 1.34 eV under AM 1.5 solar spectrum [11,12]. This is mainly because nanowire synthesis, device fabrication and junction design are still far from ideal and require substantial optimization. To understand and further improve the nanowire solar cell device properties especially the electrical properties, while avoiding the complication from the average effect of large number of nanowires in array nanowire solar cells, characterization and understanding of single nanowire materials and devices are essential.

Several III-V single nanowire solar cells have been demonstrated including GaAs [13,14], InP [15,16], InGaP [17] and GaAsP [7]. Compared to other III-V nanowires, InP nanowires are favorable for solar cell applications due to their low surface recombination velocity (SRV) [1,16,18,19]. We have previously reported single axial p-i-n InP nanowire solar cells with an efficiency up to 6.5% without any surface passivation [16]. By using the electron beam induced current (EBIC) technique, the spatially-resolved electrical structure in the p-i-n nanowire was obtained and revealed that Zn (p-dopant) diffusion was significant causing degradation of the device performance. In this work, single axial n-i-p InP nanowires were grown with n-segment first followed by i- and p-segments. Since the p-segment was grown the last, it is expected that the effect of Zn diffusion may be reduced or eliminated. We also introduce cathodoluminescence (CL) spectroscopy to directly characterize p-n junction configuration, through which the electron beam acts as a highly localized excitation source [20] to offer nanoscale resolution that cannot be achieved by other optical methods such as

Peer review under responsibility of Chinese Materials Research Society.
* Corresponding author.
E-mail address: lan.fu@anu.edu.au (L. Fu).

https://doi.org/10.1016/j.pnsc.2018.01.014
Received 31 October 2017; Accepted 2 January 2018
Available online 30 March 2018
1002-0071/ © 2018 Chinese Materials Research Society. Published by Elsevier B.V. This is an open access article under the CC BY-NC-ND license (http://creativecommons.org/licenses/BY-NC-ND/4.0/).

micro-photoluminescence (PL). Although such technique has been widely used to detect heterostructures [21–23], we show for the first time that it can be used to profile the segment length of the n-i-p structure of the same material and crystal structure. More importantly this technique does not require a complex and time consuming electrode fabrication processes, providing a simple and convenient method for growth calibration and optimization. Finally horizontally lying single nanowire solar cell devices were fabricated and characterized, demonstrating an improved performance compared with p-i-n solar cells due to reduced Zn diffusion as confirmed by EBIC measurement.

2. Experimental

2.1. Nanowire growth

The axial n-i-p junction InP nanowires were synthesized by selective-area metal organic vapor phase epitaxy (SA-MOVPE) technique on a SiO_2-masked n^+-doped 111(A) InP substrate. The substrate was first prepared by electron beam lithography (EBL) and wet chemical etching with the designed pattern of a hexagonal array targeting at holes of 180 nm in diameter and 800 nm in spacing [1,16]. Then the nanowire growth was carried out in a horizontal flow MOVPE reactor (AIXTRON 200/4) at 100 mbar with H_2 as the carrier gas. Trimethylindium (TMIn) and phosphine (PH_3) were used as precursors for In and P, respectively. The growth temperature was 730 °C with a V/III ratio of 81 (flow rate of 6.07×10^{-6} mol/min for TMIn and 4.91×10^{-4} mol/min for PH_3). Silane (SiH_4) was used as n-type dopant with a flow rate of 1.01×10^{-6} mol/min, while diethylzinc (DEZn) was used as p-type dopant with a flow rate of 2.03×10^{-5} mol/min. The growth sequence was such that n-segment was firstly grown for 10 min followed by i-segment for 10 min and p-segment for 10 min.

2.2. Optical characterization

The nanowires were first mechanically transferred to a thermally oxidized p^+-Si substrate with a 300-nm SiO_2 layer and excited by a 522 nm (frequency doubled) pulsed laser with pulse width of 300 fs and repetition rate of 20.8 MHz. The laser beam was focused by a 100× (NA 0.9) focusing objective with a spot size of 0.305 μm in radius estimated by vector diffraction calculation [24]. The PL signal was first collected by a grating spectrometer and recorded by a charge-coupled device (CCD) [24]. A Si single photon avalanched diode (SPAD) and Picoharp 300 time-correlated single photon counting system (TCSPC) were used to detect PL intensity decay [24]. The time-resolved PL (TRPL) intensity decay at the peak wavelength was fitted by a single-exponential decay to extract the minority carrier lifetime [1]. In our measurements, the power was fixed at a low excitation power of 0.26 μW (1 mW average laser power equals an excitation pulse energy of 48 pJ). So the excitation power density is 4.27 $\mu J/cm^2$/pulse.

The nanowires were also mechanically transferred to a Si substrate for CL measurement in a FEI Verios 460 field emission scanning electron microscope (SEM), with a Gatan MonoCL4 Elite CL detection system that enables CL mapping and spectroscopic studies.

2.3. Single nanowire solar cell fabrication

To fabricate single horizontal nanowire solar cell devices, nanowires were first mechanically transferred to a thermally oxidized p^+-Si substrate with a 300-nm SiO_2 layer and then the electrodes were defined by EBL patterning followed by buffered HF etching to remove the surface native oxide. Finally 10 nm Ti and 220 nm Au were deposited by electron beam evaporation and Ti/Au electrodes were formed on two ends of nanowires after the lift-off process.

2.4. Single nanowire solar cell characterization

The 1 Sun @ AM1.5G current-voltage (*I-V*) measurements of the nanowire solar cells were performed using an Oriel Solar Simulator (Mode-92250A). EBIC measurements on the fabricated devices were carried out by a FEI Helios 600 NanoLab DualBeam focused ion beam (FIB) system that allows for high resolution SEM imaging (~ 0.9 nm). Then the devices were characterized by 2-dimensional (2D) reflection and photocurrent mappings using a WITec alpha300S scanning microscopy system. Light at 532 nm from a Fianium WhiteLase supercontinuum laser was focused using a 100×, NA0.9 objective lens and then scanned across the sample using a piezo-driven sample stage. The spot size was estimated to be 721 nm in diameter. The photocurrent was measured using the conventional amplitude modulation technique with an Agilent 33210A 10MHz function/arbitrary waveform generator with a frequency of 333 Hz, Stanford SR570 low-noise current preamplifier, and Stanford SR850 lock-in amplifier. The reflected light was simultaneously detected by a confocal microscope and a Si avalanche photo-diode (APD).

3. Results and discussion

The 10° tilted SEM image of the as-grown InP nanowire array is displayed in Fig. 1a, showing good surface morphology and relatively uniform lengths (~ 7-8 μm). However, some deviation from perfect hexagonal cross-section is observed in the top-view SEM image (inset of Fig. 1a) due to the relatively large nanowire spacing (800 nm) and consequent non-uniform lateral growth [1,16]. As confirmed by the *I-V* characteristics shown in Fig. 3b, the lateral growth is insignificant such that it does not lead to the formation of a conformal radial junction.

To investigate the optical properties of n-, i- and p-segments, we measured PL and TRPL from the n-i-p nanowires at room temperature. The PL intensity and TRPL decays with the fitting from three positions of the n-, i- and p-regions are displayed in Fig. 1b and c. The minority

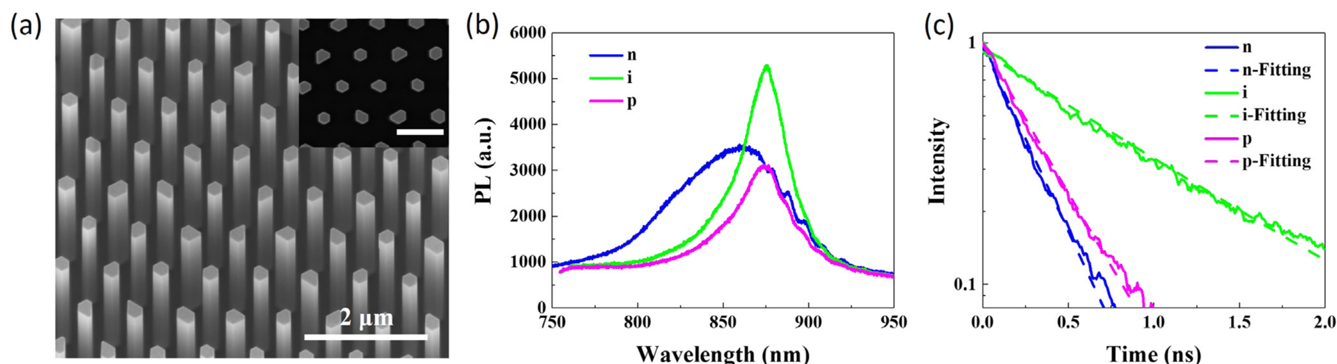

Fig. 1. (a) SEM image at 10° tilt view of the InP nanowire array grown for this work. Inset shows the top view SEM image. The scale bar of the inset is 1 μm. (b) PL and (c) TPRL decays with fittings of n-, i- and p-regions, respectively.

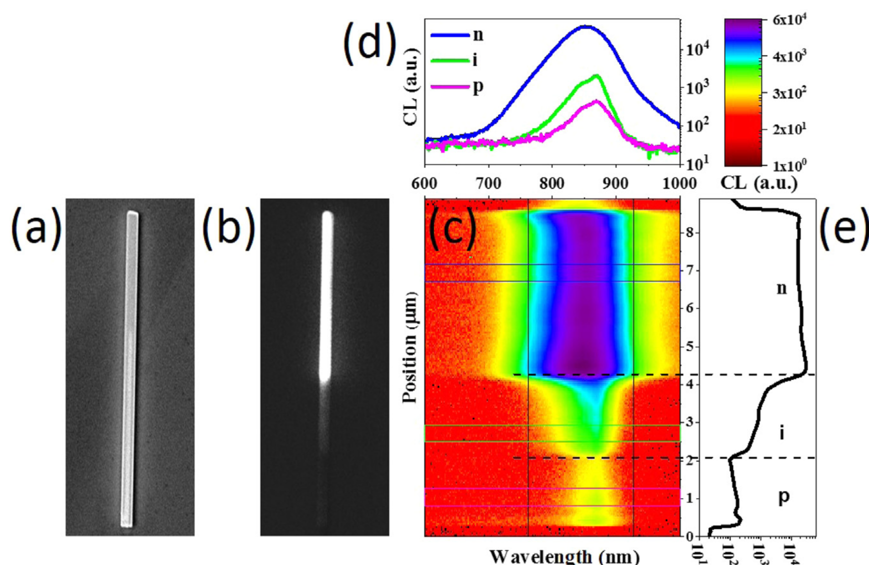

Fig. 2. (a) Secondary electron and (b) panchromatic CL image with corresponding (c) full spectral CL line scan along the nanowire length, (d) CL spectra for the n-, i- and p-regions indicated in c and (e) CL intensity profile along the nanowire extracted from the line scan.

carrier lifetimes of the three positions were also extracted from the TRPL decay fitting as 0.28, 0.96 and 0.35 ns, respectively. As clearly seen, the PL peak from n-region is blue-shifted and broadened compared to that from the i- and p-regions due to the Burstein-Moss shift [25]. Based on our previous study [24], the doping concentration of n-region under the current growth condition is $\sim 3 \times 10^{18}$ cm^{-3}. The i-region shows the longest lifetime of 0.96 ns at the PL peak wavelength, indicating the least contamination and lattice defects introduced by the n- and p-type doping during the growth [26]. Unlike reported in Ref. [27], where large PL redshift has been observed in p-doped InP nanowires, the PL peak measured from the p-type region of our n-i-p nanowires does not show any shift from the i-region, however with a much reduced intensity and carrier lifetime, which may be due to the relatively low p-doping concentration typically obtained in our nanowires grown by selective-area epitaxy (SAE) method [28–30].

Fig. 2 shows a CL spectral line scan from a typical n-i-p nanowire, collected at room temperature with an accelerating voltage of 3 kV and beam current of 100 pA. From the line scan in Fig. 2e, three distinct regions can be identified. From the spectra shown in Fig. 2d that were extracted from the map in Fig. 2c, we can identify these regions as the n-, i- and p-segments, based on the blue-shifted and broadened CL peak of n-region compared to that of i- and p-regions. Moreover, the n-region shows a much stronger luminescence than the other two regions. This is mainly due to the increased doping level in the n-region and the increased transition probability for a donor-valence band transition compared to a conduction band-valence band transition [31]. Fig. 2e shows the total CL intensity along the length of the nanowire, calculated from the line scan, which shows that the n-region is much longer that the p- and i-regions. From the line scan we can estimate that the average growth rates in n-, i- and p-segments are approximately 7.5, 3.3 and 3.2 nm/s, respectively, and this is consistent with the fact that our nanowire growth rate decreases as the growth progresses. For SAE growth, the initial growth typically shows significantly high growth rate since most adatoms on the oxide mask are able to diffuse to the top of the nanowire and participate in axial growth. As nanowire becomes longer beyond the diffusion length of the adatoms, they cannot reach the top of the nanowire and hence do not contribute to additional axial growth. From Fig. 2e we can see that the CL intensity across the i-segment is not uniform, which could be a result of carrier diffusion during the CL measurement and/or some n and p dopant diffusion during the nanowire growth.

Fig. 3a illustrates the schematic of the n-i-p nanowire solar cell device. The *I-V* characteristics measured from the best nanowire device in dark and under 1 Sun @ AM1.5G illumination condition are shown in Fig. 3b, exhibiting a typical photovoltaic (PV) behavior. Based on the top view SEM measurement (0° tilt) of the nanowire's projected area (product of nanowire uncontacted length and diameter), a short circuit current density (J_{sc}) of 12.62 mA/cm^2, open circuit voltage (V_{oc}) of 0.88

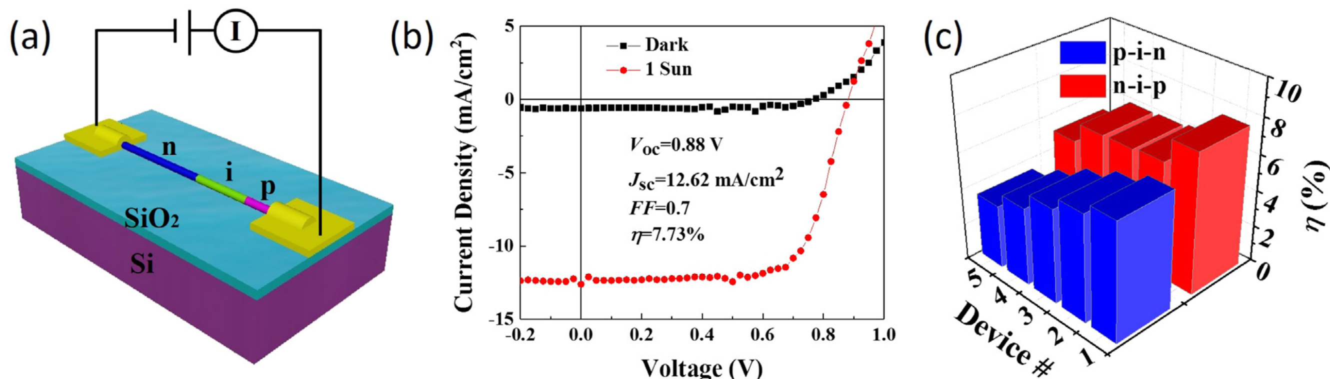

Fig. 3. (a) Schematic illustration of a single horizontal n-i-p InP nanowire solar cell. (b) *I-V* characteristics under dark (black curve) and 1 Sun @ AM1.5G illumination (red curve) conditions of the fabricated solar cell. (c) PCE comparison of p-i-n [16] and n-i-p single nanowire solar cells.

Table 1
Summary of key performance parameters of six InP single nanowire solar cells.

	V_{oc} (V)	J_{sc}(mA/cm^2)	*FF*	η (%)
Device 1	0.88	12.62	0.7	7.73
Device 2	0.82	11.47	0.676	6.4
Device 3	0.86	9.53	0.765	6.27
Device4	0.85	10.76	0.68	6.22
Device 5	0.8	10.82	0.59	5.11
Device 6	0.78	9.7	0.66	5

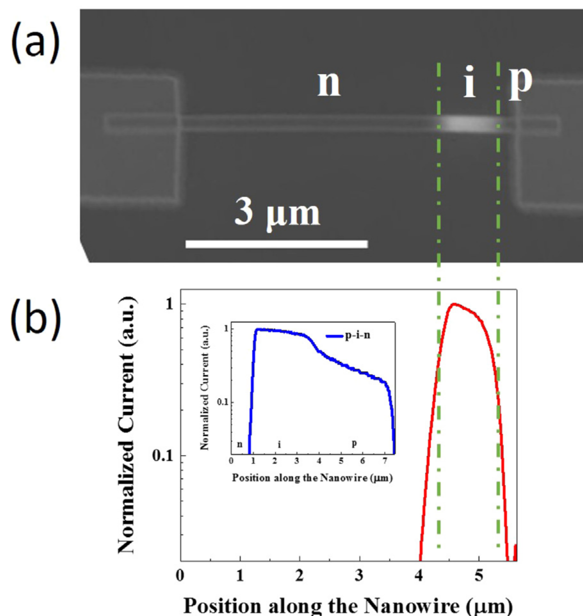

Fig. 4. (a) SEM image and EBIC response (overlaid) of the InP nanowire solar cell. (b) EBIC intensity profile along the center of the nanowire. Inset: EBIC intensity profile along the center of a p-i-n nanowire solar cell for reference [16].

V and fill factor (*FF*) of 0.7 were obtained from the device leading to a cell efficiency (η) of 7.73%, under the 1Sun@AM1.5G illumination. Table 1 summarizes the key device parameters of six nanowire solar cells. Also the PCE comparison of reported p-i-n [16] and our n-i-p single nanowire solar cells is shown in Fig. 3c. Compared with the unpassivated p-i-n junction InP nanowire solar cells reported previously, the n-i-p solar cells show similar V_{oc} but improved J_{sc} and *FF*, leading to overall higher PCEs.

The EBIC measurements were also carried out for the fabricated devices. Fig. 4a shows the SEM image and the corresponding EBIC response (overlaid) from the single n-i-p nanowire device. The EBIC profile along the nanowire is displayed in Fig. 4b. Since the nanowire device was unbiased, the EBIC signal originated from the locally generated electron-hole pairs (excited by the electron beam) within the depletion region, as well as the ones generated outside but within the diffusion length of the minority carriers [16], and their subsequent separation by the built-in field. The EBIC image agrees well with the CL map and presents three segments with clear contrasts: a long and dark region close to the n-contact, a bright segment representing the i-region where a built-in electric field is expected to form leading to a large drift current under the electron beam excitation, and a short and dark p-region which is mostly covered by the contact. Correspondingly, the plateau region of the EBIC intensity profile in Fig. 4b with the highest intensity indicates that the i-region of the n-i-p structure has a low background doping concentration. The "sharp" drop of the EBIC intensity from either side of the i-region to almost zero indicates that not much carrier diffusion occurred in both n- and p-segments, which could be due to their high doping concentrations. This is in stark contrast to the EBIC profile obtained from the p-i-n structure, as shown in the inset of Fig. 4b as a reference, which presents a highly asymmetrical and gradual slope towards the p-contact region as a result of significant Zn diffusion. This result suggests that altering the growth sequence from p-i-n to n-i-p can effectively suppress the Zn diffusion, leading to more intrinsic i-region, higher doping concentration of the p-region and thus, improved device performance.

Fig. 5 presents the optical image, 2D reflection and photocurrent maps of the single n-i-p nanowire solar cell measured under a 532 nm laser excitation at zero bias. As indicated by the white dotted circle in Fig. 5c, the spatial distribution of the photocurrent corresponds very well to that of the un-contacted exposed part of the nanowire as

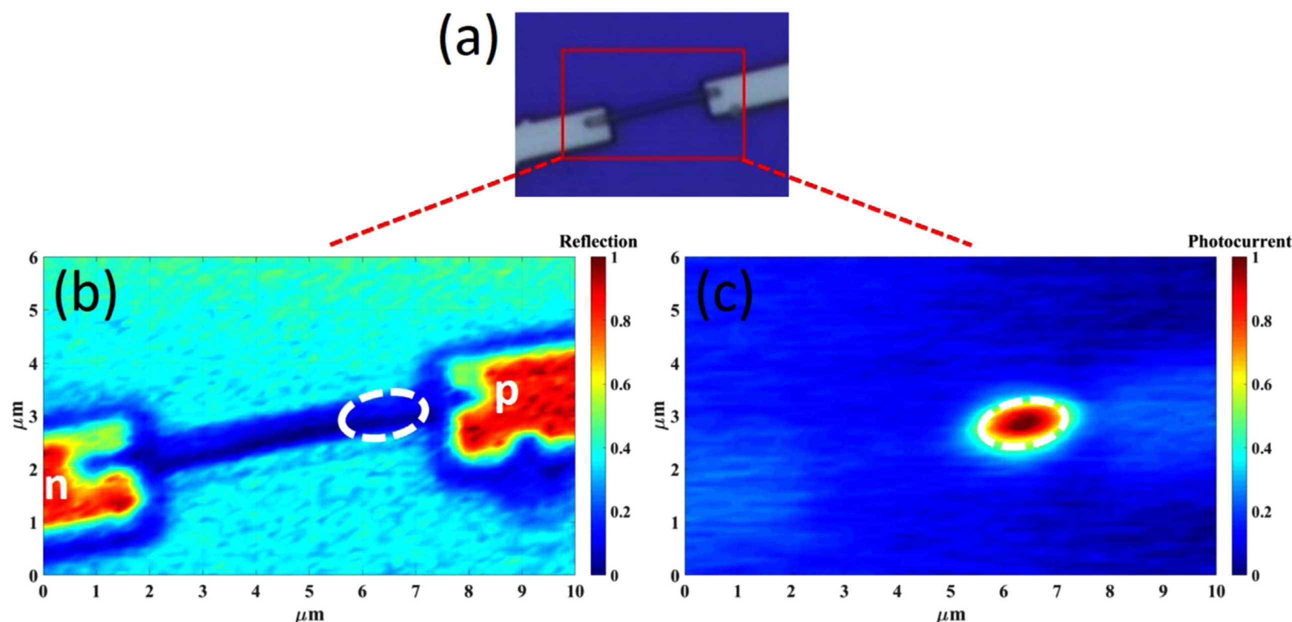

Fig. 5. (a) Optical image, (b) 2D reflection and (c) photocurrent maps of the fabricated nanowire solar cell presented in Fig. 4 under 532 nm laser excitation with no bias voltage.

indicated by the white dotted circle in the reflection map in Fig. 5b. This means that the zero bias photocurrent originates from the depletion region, ruling out the possibility of Schottky junction related PV behavior. Combined with *I-V* measurement, we confirm the n- and p-sides of the device and found that the length of n-segment is more than half of the whole length, corresponding well with the CL and EBIC intensity profiles. Different from the photocurrent mapping result observed from the p-i-n nanowire solar cell [16] where a weak photocurrent in the long segment along the nanowire was generated from the p-region due to carrier diffusion, the n-i-p device does not show much carrier diffusion from either side of the junction.

Based on the above CL, EBIC and 2D photocurrent mapping results, it is clear that the efficiency of our axial n-i-p nanowire solar cells may be further enhanced by the optimization of structure design and growth conditions. For example, it is shown that due to the non-uniform growth rate during the nanowire growth, the 10 min growth time resulted in much longer n-segment compared with the i- and p-segments. Since the n-segment has high doping concentration to serve only as a contact region with little contribution to the photocurrent, its length can be largely decreased by reducing the growth time. The i-region generated the highest EBIC current as well as the photocurrent. However its current length is very short which could be further optimized to maximize absorption while maintain sufficient built-in electric field for efficient carrier collection. Due to the very short p-segment it may be helpful to slightly increase the p-segment length to ensure sufficient contact region and avoid contacting of i-region. Nevertheless, compared with axial p-i-n junction, we believe that n-i-p sequence is more preferable for nanowire solar cell growth due to the suppressed Zn-diffusion, leading to higher efficiency and less complicated junction optimization.

4. Conclusions

In this work, axial n-i-p junction InP nanowires were grown by SA-MOVPE technique. The CL mapping technique was used for the first time to obtain the dimensional information of the axial n-i-p junction formed by the same material and crystal structure. The fabricated InP single nanowire solar cells have been demonstrated with PCE up to 7.73% with suppressed Zn diffusion from the p-segment. A series of nano-scale characterization techniques on the solar cells were employed to further reveal the origin of the photocurrent, critical for future device optimization. Our work suggests that the bottom up growth sequence of n-i-p junction is a preferred design to achieve high performance nanowire solar cells.

Acknowledgments

The authors acknowledge the Australian Research Council (ARC) for financial support and the Australian National Fabrication Facility (ANFF) ACT node for facility support.

References

[1] Q. Gao, D. Saxena, F. Wang, L. Fu, S. Mokkapati, Y. Guo, L. Li, J. Wong-Leung, P. Caroff, H.H. Tan, Nano Lett. 14 (2014) 5206–5211.
[2] D. Saxena, S. Mokkapati, P. Parkinson, N. Jiang, Q. Gao, H.H. Tan, C. Jagadish, Nat. Photonics 7 (2013) 963–968.
[3] Z. Li, X. Yuan, L. Fu, K. Peng, F. Wang, X. Fu, P. Caroff, T.P. White, H.H. Tan, C. Jagadish, Nanotechnology 26 (2015) 445202.
[4] K. Peng, P. Parkinson, L. Fu, Q. Gao, N. Jiang, Y.-N. Guo, F. Wang, H.J. Joyce, J.L. Boland, H.H. Tan, Nano Lett. 15 (2014) 206–210.
[5] S. Maeda, K. Tomioka, S. Hara, J. Motohisa, Jpn. J. Appl. Phys. 51 (2012) 02BN03.
[6] E.D. Minot, F. Kelkensberg, M. Van Kouwen, J.A. Van Dam, L.P. Kouwenhoven, V. Zwiller, M.T. Borgström, O. Wunnicke, M.A. Verheijen, E.P. Bakkers, Nano Lett. 7 (2007) 367–371.
[7] J.V. Holm, H.I. Jørgensen, P. Krogstrup, J. Nygård, H. Liu, M. Aagesen, Nat. Commun. 4 (2013) 1498.
[8] J. Wallentin, N. Anttu, D. Asoli, M. Huffman, I. Åberg, M.H. Magnusson, G. Siefer, P. Fuss-Kailuweit, F. Dimroth, B. Witzigmann, Science 339 (2013) 1057–1060.
[9] I. Aberg, G. Vescovi, D. Asoli, U. Naseem, J.P. Gilboy, C. Sundvall, A. Dahlgren, K.E. Svensson, N. Anttu, M.T. Bjork, IEEE J. 6 (2016) 185–190.
[10] D. Van Dam, N.J. Van Hoof, Y. Cui, P.J. Van Veldhoven, E.P. Bakkers, J. Gómez Rivas, J.E. Haverkort, ACS Nano 10 (2016) 11414–11419.
[11] N. Anttu, ACS Photonics 2 (2015) 446–453.
[12] S. Mokkapati, C. Jagadish, Optics Express 24 (2016) 17345–17358.
[13] C. Colombo, M. Heiβ, M. Grätzel, A. Fontcuberta, I. Morral, Appl. Phys. Lett. 94 (2009) 173108.
[14] N. Han, F. Wang, S. Yip, J.J. Hou, F. Xiu, X. Shi, A.T. Hui, T. Hung, J.C. Ho, Appl. Phys. Lett. 101 (2012) 013105.
[15] A. Nowzari, M. Heurlin, V. Jain, K. Storm, A. Hosseinnia, N. Anttu, M.T. Borgstro¨m, Hk Pettersson, L. Samuelson, Nano Lett. 15 (2015) 1809-–11814.
[16] Z. Zhong, Z. Li, Q. Gao, Z. Li, K. Peng, L. Li, S. Mokkapati, K. Vora, J. Wu, G. Zhang, Nano Energy 28 (2016) 106–114.
[17] C. Gutsche, A. Lysov, D. Braam, I. Regolin, G. Keller, Z.A. Li, M. Geller, M. Spasova, W. Prost, F. J, Adv. Funct. Mater. 22 (2012) 929–936.
[18] G. Otnes, M.T. Borgström, Nano Today 12 (2016) 31–45.
[19] H.J. Joyce, J. Wong-Leung, C.-K. Yong, C.J. Docherty, S. Paiman, Q. Gao, H.H. Tan, C. Jagadish, J. Lloyd-Hughes, L.M. Herz, Nano Lett. 12 (2012) 5325–5330.
[20] B.J. Brenny, D.R. Abujetas, D. van Dam, J.A. Sánchez-Gil, J.Gm Rivas, A. Polman, ACS Photonics 3 (2016) 677–684.
[21] D. Lindgren, M. Heurlin, K. Kawaguchi, M. Borgström, M.-E. Pistol, B. Monemar, L. Samuelson, A. Gustafsson, J. Phys.: Conf. Ser. 471 (2013) 012040.
[22] A. Gustafsson, J. Bolinsson, N. Sköld, L. Samuelson, Appl. Phys. Lett. 97 (2010) 072114.
[23] J. Bolinsson, M. Ek, J. Trägårdh, K. Mergenthaler, D. Jacobsson, M.-E. Pistol, L. Samuelson, A. Gustafsson, Nano Res. 7 (2014) 473–490.
[24] F. Wang, Q. Gao, K. Peng, Z. Li, Z. Li, Y. Guo, L. Fu, L.M. Smith, H.H. Tan, C. Jagadish, Nano Lett. 15 (2015) 3017–3023.
[25] J. Wallentin, M.T. Borgström, J. Mate. Res. 26 (2011) 2142–2156.
[26] H. Xia, Z.-Y. Lu, T.-X. Li, P. Parkinson, Z.-M. Liao, F.-H. Liu, W. Lu, W.-D. Hu, P.-P. Chen, H.-Y. Xu, ACS Nano 6 (2012) 6005–6013.
[27] M. Van Weert, O. Wunnicke, A. Roest, T. Eijkemans, A. Yu Silov, J. Haverkort, G. t Hooft, E. Bakkers, Appl. Phys. Lett. 88 (2006) 043109.
[28] W. Zhang, S. Lehmann, K. Mergenthaler, J. Wallentin, M.T. Borgstro¨m, M.-E. Pistol, A. Yartsev, Nano Lett. 15 (2015) 7238-–77244.
[29] W. Zhang, F. Yang, M.E. Messing, K. Mergenthaler, M.-E. Pistol, K. Deppert, L. Samuelson, M.H. Magnusson, A. Yartsev, Nanotechnology 27 (2016) 455704.
[30] F. Ishikawa, I. Buyanova, Novel Compound Semiconductor Nanowires: Materials, Devices, and Applications, CRC Press, 2017.
[31] J. Pankove, Optical Processes in Semiconductors. 1971, New York.